Analysis and Experimental Verification of the Strength of Telescopic Booms for Construction Machinery

[1]Zhe CUI, [1]Wenguang JIANG*, [2]Lei CHENG

[1]*School of Mechanical Engineering*, Yanshan University, Qinhuangdao, Hebei, 066004, China
[2]XCMG Xuzhou Environmental Technology Co.,Ltd, Xuzhou, Jiangsu, 221000, China

***Abstract* — Telescopic booms are key elements for payload lifting in construction machineries. They usually consist of thin-walled hollow segments that can retract, extend or elevate during operation. The mechanical properties of the telescopic booms directly determine the lifting capacity of these machines. The overlapping contact regions between the adjacent booms are critical locations where high stresses occur, thus the stress level in these regions is the key factor representing the strength of the telescopic boom structures. According to the principle of superposition, a mathematical model has been proposed for analysis of stresses in the contact zones of telescopic boom structure. The proposed model calculates the global bending stress according to the beam bending theory, then uses a partial telescopic boom geometry isolated from the contact zones to establish a local analytical model to determine the local stresses according to the plate bending theory, and finally superimposes the two states of stresses to obtain the final stress state which represents the strength of the telescopic booms. The proposed analytical model has been validated by both finite element analysis and experimental test conducted on a telescopic aerial platform.**

Keywords - telescopic boom; structural strength; principle of superposition; bending stress; analytical model; experimental verification.

I. INTRODUCTION

Telescopic booms in construction machineries conduct payload lifting task by retracting, extending or elevating. They are usually the direct loading bearing parts in the whole system of the machinery, as shown in Fig.1. Reducing the selfweight of the telescopic booms could help increase the effective payload lifting capacity, and increase the lifting and extension operation speeds of the booms as well. In recent years, manufacturers have paid more and more attention on the sectional shape selection and optimization of the telescopic booms. The consequence of using these optimized section design can not only reduce the weight of the telescopic booms, but also increase the bending stiffness and torsion stiffness in the same time[1,2]. During maintenance or repair, plastic deformation and cracks could often be observed in the vicinity of the overlap contact regions between two adjacent telescopic booms. This indicates that the stresses within these regions are much higher than other regions.

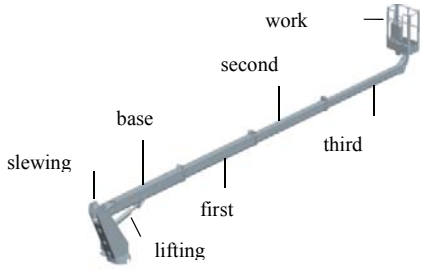

Figure 1. Structure of the telescopic boom

The studies of the stress distributions within the overlapping contact region of telescopic booms have been reported by several researchers. Based on the results of static strength experiment on the rectangular cross-sectional telescopic boom overlapping structure, Liu and Wang [3] proposed a stress expression using superposition of three analytical solutions of simply supported plate models under different loading conditions. The predicted stresses from this model were validated by experimental results. Djelosevic et al.[4] studied the effect of local stress on the carrying capacity and optimum design of box girders. Savkovic et al. [5] studied the local stress increases at the overlapping contact regions of rectangular telescopic booms of truck cranes.

With the development of modern computing technology, the finite element methods are widely used to perform numerical analyses for the telescopic boom structure. Numerical solutions of the stress distributions could be obtained and structural optimizations could be carried out based on the stress analysis results [6-8]. Some of them used the nodal degrees of freedom coupling technology to connect each booms. Some used contact analysis capability of software to solve stresses on the contact areas of the telescopic booms. As there exist many complex contact regions on the telescopic boom structures and it is a well know problem that the contact stress analysis processes are highly nonlinear, finite element modelling of these structures are normally very time-consuming, and in many cases, convergence difficulties are often encountered during analyses. These factors limit the wide application of the finite element analyses to the telescopic boom structures.

Compare to finite element models, analytical models are very efficient to run. However most of the existing analytical models for telescopic boom structures have poor stress prediction accuracy due to the use of the oversimplified

assumptions that the contacts occur over the entire sliding surface of the sliding blocks. In the current study, it has been found from the elaborately conducted finite element analysis results that the transfer of loads between the overlapping contact booms are actually realized through very narrow contacting areas along the edges of the sliding blocks, rather than the whole sliding surface of the sliding blocks. Based on the observation, we could make a rational assumption that the distribution of contact load transferred between contacting booms is along the narrow edge areas of the sliders. Using this more realistic assumption and the principle of superposition for elastic structures, in this paper, a new mathematical model for the determination of critical stresses in the contact regions has been proposed by superimposing the structural global bending normal stress with the local transverse bending stress in the contact zone.

II. STRESS ANALYSIS IN THE BOOM CONTACT REGIONS

The telescopic boom structure is usually composed of two or more hollow-sectioned booms nesting together one after another. The inner booms can slide within the outer neighboring booms. The loads transferred between the neighboring booms are realized through the sliding contacts between the sliding blocks and the sliding surfaces of the booms. The upper sliding blocks are fixed on top of the out-surface at the end of the inner boom, and the lower sliding blocks are fixed on the lower inner surface of the out boom, see Fig.3. The load transferring mechanism is illustrated in Fig.4. In this paper, the analytical solution of the critical stress within the contact regions of the telescopic boom system with nesting hexagonal cross-sections are studied in detail. Fig.2 shows the parametric dimensions of the hexagonal boom cross-sections. H is the height of the boom cross section, W the width of the boom cross section, T the plate thickness, H1 the height of the web plate, W1 the width of the bottom flange plate, and α1 the inclined angle of the web plate.

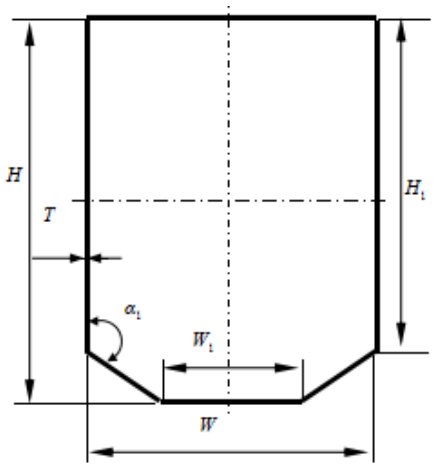

Figure 2. Cross-section of the telescopic boom

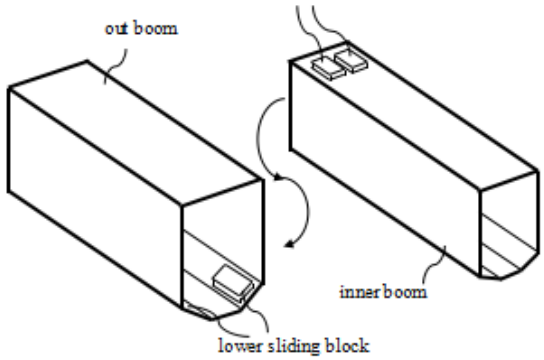

Figure 3. Sliding blocks locations on the out and inner booms.

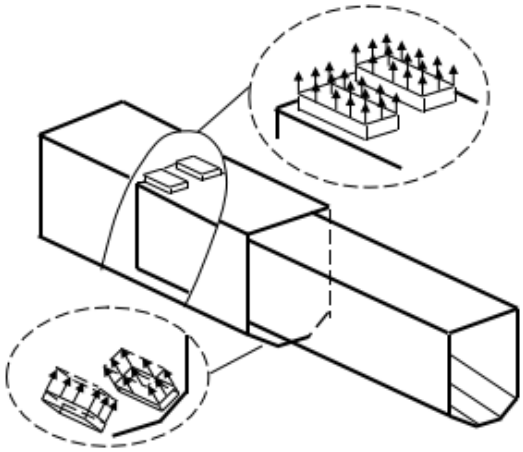

Figure 4. Load transfer via sliding blocks

Within the regime of elastic deformation, the stress in the contact area can be considered as the superposition of two states of stresses. The first part is the normal bending stress caused by the global bending deformation of the boom. The second part is the local bending stress caused by the transverse local bending deformation. The former is shown in Fig.5, and the latter is shown in Fig.6.

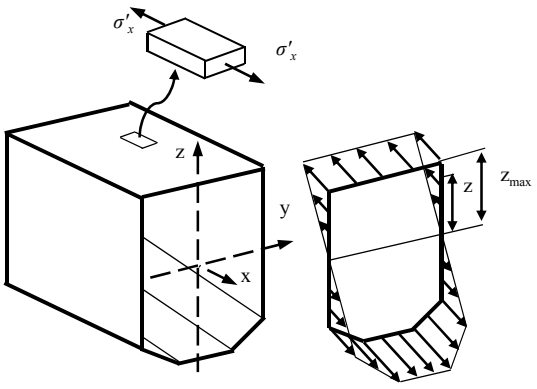

Figure 5. Global bending normal stress

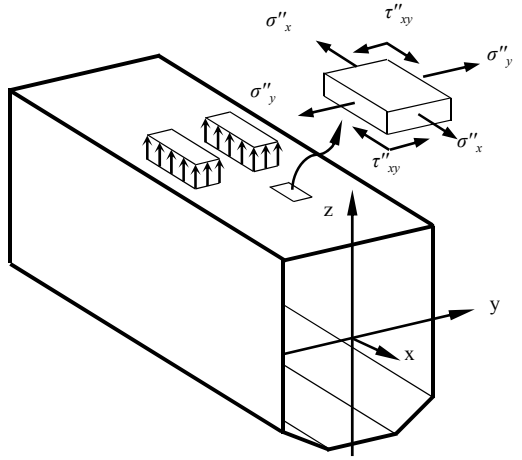

Figure 6. Local bending stress

The final resultant stress components σx, σy, and τxy in the contact region can be calculated as the summation of the corresponding stress components of the global bending stress and the local transverse bending stress:

$$\sigma_x = \sigma_x^{'} + \sigma_x^{"} \tag{1}$$

$$\sigma_y = \sigma_y^{"} \tag{2}$$

$$\tau_{xy} = \tau_{xy}^{"} \tag{3}$$

where x is the direction along the boom length, y the transverse direction of the plate as shown in Fig.5 and Fig.6.

A. The Global Bending Normal Stress

Provided that n is the total number of booms in the whole telescopic boom system. The diagram of forces on a portion of the telescopic boom system from ith boom to the nth boom is shown in Fig.7.

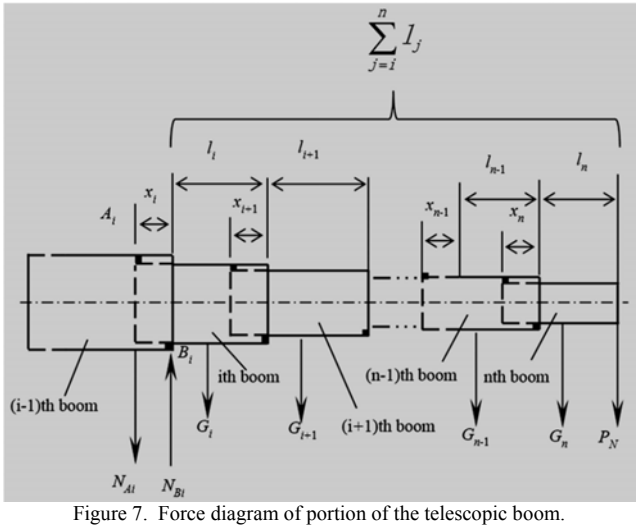

Figure 7. Force diagram of portion of the telescopic boom.

l_i is the stretch-out length of the *i*th boom. x_i is the overlapping length between the neighboring *i*th boom and the (*i*+1)th boom. G_i is the self weight of *i*th boom. Assuming the self weight of each boom is uniformly distributed along its length, the location of center of self weight should be on the midpoint of each boom. The payload P_N is exerted on the tip of the *n*th boom, refer to Fig.7. The two contact action points on *i*th boom are designated as A_i and B_i , where *A* indicates the left side point, *B* is the right side point, and *i* is the boom number.

Considering equilibrium of both force and moment, the balance forces transferred from the (*i*-1)th boom to the ith boom at the contact points are given as:

$$N_{Ai} = [\sum_{j=i}^{n} G_j (l_j - x_j) + 2\sum_{j=i+1}^{n} G_j \sum_{k=i}^{j-1} l_k + 2P_N \sum_{j=i}^{n} l_j] / 2x_i \tag{4}$$

$$N_{Bi} = [\sum_{j=i}^{n} G_j (l_j + x_j) + 2\sum_{j=i+1}^{n} G_j \sum_{k=i}^{j-1} l_k + 2P_N \sum_{j=i}^{n} l_j] / 2x_i + P_N \tag{5}$$

Using equations (4) and (5), the balancing forces on all booms can be calculated, the bending moment M_i on any cross-section of the booms can be obtained, and the bending normal stress $\sigma_x^{'}$ can also be calculated by using the following equation:

$$\sigma_x^{'} = \frac{M_i}{I_i} Z \tag{6}$$

where I_i is the moment of inertia of the ith boom cross-section with respect to the y-axis.

B. The Local Bending Stress

As the thickness of the plates of the boom is much smaller than the width and length of the plates, the theory of elastic thin walled plate could be applied to solve the local bending problem of the plates. The stress components $\tau_{zx}^{"}$, $\tau_{zy}^{"}$ and $\sigma_z^{"}$ are very small and could thus be safely ignored, compared to the other three major stress components.

The contact stress had been usually assumed to be uniformly distributed on the sliding contacting surfaces of the sliding block when developing analytical solutions to the problem. However, from our study using accurate full three dimensional finite element analysis, contacts were found to occur only along the narrow edge regions of the sliding block, and the width of the contacting regions is about twice the thickness of the contacting plates. The reason for this is mainly due to the local bending deformation as illustrated in Fig.8. Based on these findings, the analytical theory developed in this paper using a more realistic hypotheses which assume that contacts between the neighbouring booms occur along the narrow edge regions of the sliding blocks,

the width of the narrow contact regions is twice the thickness of the plates and the contact loads are uniformly distributed within these narrow regions.

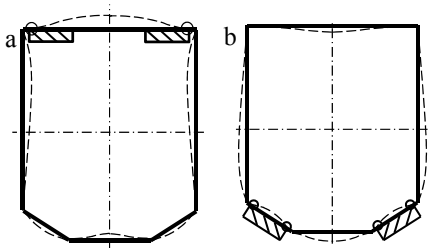

Figure 8. Local bending deformation of the cross- section at the contact zone of the telescopic booms: out boom (left) and inner boom (right).

Consider a singled-out portion of the booms with a length of a (a = 2*H*， a is much greater than the length of the contact slider, see Fig.9). For the convenience of analysis, the boom portions could be further disassembled to six smaller sub-portions, i.e. (1) top flange, (2) right web, (3) right inclined plate, (4) bottom flange, (5) left inclined plate, and (6) left web, see Fig. 10. These disassembled plates are analyzed as simply supported plates subjected to bending moments, and the same bending moments are applied to both sides of the disassembled edges, see Fig. 10.

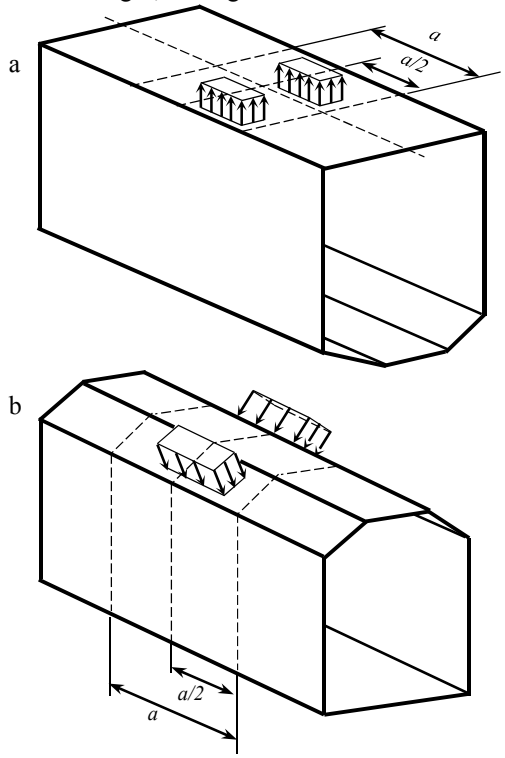

Figure 9. The portion of boom loaded via sliding blocks: out boom (top) and inner boom (bottom)

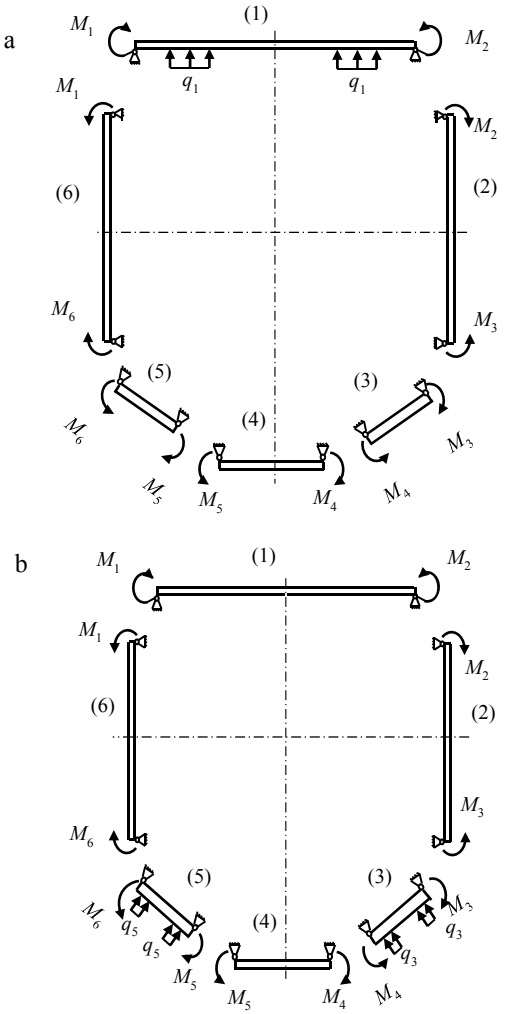

Figure 10. Model for analysis: out boom (top) and inner boom (bottom).

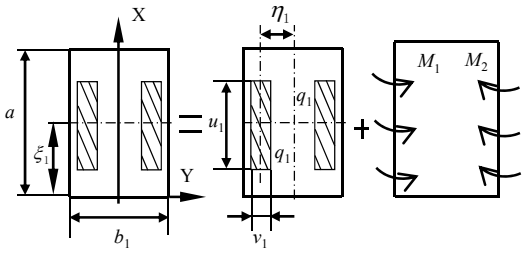

Figure 11. Superposition of the loads for the top flange plate

The differential equation for the transversely loaded plate has the form [12]

$$\frac{\partial^4 w}{\partial x^4} + 2\frac{\partial^4 w}{\partial x^2 y^2} + \frac{\partial^4 w}{\partial y^4} = \frac{q(x,y)}{D} \tag{7}$$

where:

$D = \dfrac{E\delta^3}{12(1 \pm \mu^2)}$ is the bending stiffness of the plate.

E is Young's modulus. μ is Poisson ratio. δ is the thickness of the plate.

The deflection of simply supported plate due to uniform continuous load q is:

$$w(q)=\frac{16q}{\pi^6 D}\sum_{m=1}^{\infty}\sum_{n=1}^{\infty}\frac{\sin\frac{m\pi\zeta}{a}\sin\frac{n\pi\eta}{b}}{mn(\frac{m^2}{a^2}+\frac{n^2}{b^2})^2}\times\sin\frac{m\pi u}{2a}\sin\frac{n\pi v}{2b}\sin\frac{m\pi x}{a}\sin\frac{n\pi y}{b} \tag{8}$$

The inclination of this plate due to the load q is given by the expression:

$$\frac{\partial w(q)}{\partial y}=\frac{16q}{\pi^5 Db}\sum_{m=1}^{\infty}\sum_{n=1}^{\infty}\frac{\sin\frac{m\pi\zeta}{a}\sin\frac{n\pi\eta}{b}}{m(\frac{m^2}{a^2}+\frac{n^2}{b^2})^2}\times\sin\frac{m\pi u}{2a}\sin\frac{n\pi v}{2b}\sin\frac{m\pi x}{a}\cos\frac{n\pi y}{b} \tag{9}$$

The deflection of simply supported plate due to the action of moments Mi and M_{i+1} is:

$$\begin{aligned}w_i(M_i,M_{i+1})=&\frac{a^2}{4D_i\pi^2}\sum_{m=1}^{\infty}\frac{1}{m^2}[\frac{E_{im}+E_{(i+1)m}}{\cosh\alpha_{im}}\\&\times(\alpha_{im}\tanh\alpha_{im}\cosh\frac{m\pi y}{a}-\frac{m\pi y}{a}\sinh\frac{m\pi y}{a})\\&+\frac{E_{(i+1)m}-E_{im}}{\sinh\alpha_{im}}\times(\alpha_{im}\coth\alpha_{im}\sinh\frac{m\pi y}{a}-\\&\frac{m\pi y}{a}\cosh\frac{m\pi y}{a})]\sin\frac{m\pi x}{a}\end{aligned} \tag{10}$$

The moment M_i , M_{i+1} and α_{im} are determined according to the following series:

$$M_i=\sum_{m=1}^{\infty}E_{im}\sin\frac{m\pi x}{a}$$

$$M_{i+1}=\sum_{m=1}^{\infty}E_{(i+1)m}\sin\frac{m\pi x}{a}$$

$$\alpha_{im}=\frac{m\pi b_i}{2a}$$

where E_{im} and $E_{(i+1)m}$ are unknown coefficients.

The corresponding inclinations of the plate at Y=±b/2 are determined using the expressions:

$$\left.\frac{\partial w_i(M_i,M_{i+1})}{\partial y_i}\right|_{y=\frac{-b_i}{2}}=\frac{a}{4D_i\pi^2}\sum_{m=1}^{\infty}\frac{1}{m}[-(E_{im}+E_{(i+1)m})F_{im}+(E_{(i+1)m}-E_{im})H_{im}]\sin\frac{m\pi}{a} \tag{11}$$

$$\left.\frac{\partial w_i(M_i,M_{i+1})}{\partial y_i}\right|_{y=\frac{b_i}{2}}=\frac{a}{4D_i\pi}\sum_{m=1}^{\infty}\frac{1}{m}[(E_{im}+E_{(i+1)m})F_{im}+(E_{(i+1)m}-E_{im})H_{im}]\sin\frac{m\pi}{a} \tag{12}$$

The coefficients Fim and Him are given through the following expressions:

$$F_{im}=-(\frac{\alpha_{im}}{\cosh^2\alpha_{im}}+\tanh\alpha_{im})$$

$$H_{im}=(\frac{\alpha_{im}}{\sinh^2\alpha_{im}}-\coth\alpha_{im})$$

As shown in Fig. 10 (a)，the top flange plate of the out boom is mutually subjected to the local distributed loads and the bending moments. By using the principle of superposition, the analysis of the top flange of the out boom can be considered as the superposition of the two simpler loading cases as shown in Fig.11.

For the loading case of the top flange plate being considered as simply supported plate subjected to the local uniform continuous load q1, the deflection can be obtained from formula (8):

$$w_1(q)=\frac{16q_1}{\pi^6 D_1}\sum_{m=1}^{\infty}\sum_{n=1}^{\infty}\frac{\sin\frac{m\pi\zeta_1}{a}\sin\frac{n\pi\eta_1}{b_1}}{mn(\frac{m^2}{a^2}+\frac{n^2}{b_1^2})^2}\times\sin\frac{m\pi u_1}{2a}\sin\frac{n\pi v_1}{2b_1}\sin\frac{m\pi x}{a}\sin\frac{n\pi y}{b_1} \tag{13}$$

For the loading case of the top flange being considered as simply supported plate subjected to distributed bending moment M_1 and M_2 at Y= $\pm b_1/2$, the deflection can be obtained from formula (10):

$$\begin{aligned}w_1(M_1,M_2)=&\frac{a^2}{4D_1\pi^2}\sum_{m=1}^{\infty}\frac{1}{m^2}[\frac{E_{1m}+E_{2m}}{\cosh\alpha_{1m}}\\&\times(\alpha_{1m}\tanh\alpha_{1m}\cosh\frac{m\pi y}{a}-\frac{m\pi y}{a}\sinh\frac{m\pi y}{a})\\&+\frac{E_{2m}-E_{1m}}{\sinh\alpha_{1m}}\times(\alpha_{1m}\coth\alpha_{1m}\sinh\frac{m\pi y}{a}-\\&\frac{m\pi y}{a}\cosh\frac{m\pi y}{a})]\sin\frac{m\pi x}{a}\end{aligned} \tag{14}$$

By superimposing Eq. (13) and Eq. (14), we have the deflection equation of the upper wing plate:

$$w_1=w_1(q)+w_1(M_1,M_2) \tag{15}$$

The rest of the plates can be considered as simply supported plates at all four edges, subjected to distributed bending moment M_i and M(i+1) at Y= $\pm$ $b_i/2$ sides using the Eq. (10). The deflection of equations are:

$$w_i=w_i(M_i,M_{i+1}) \tag{16}$$

In order to ensure the continuity of the deformation of the boom, the following boundary conditions must be satisfied:

$$\left.\frac{\partial w_6(M_6,M_1)}{\partial y_6}\right|_{y_6=\frac{b_6}{2}}=\left.\frac{\partial w_1(q)}{\partial y_1}\right|_{y_1=\frac{-b_1}{2}}+\left.\frac{\partial w_1(M_1,M_2)}{\partial y_1}\right|_{y_1=\frac{-b_1}{2}} \tag{17}$$

$$\left.\frac{\partial v_1(q)}{\partial y_1}\right|_{y_1=\frac{b_1}{2}} + \left.\frac{\partial v_1(M_1,M_2)}{\partial y_1}\right|_{y_1=\frac{b_1}{2}} = \left.\frac{\partial v_2(M_2,M_3)}{\partial y_2}\right|_{y_2=\frac{-b_2}{2}} \tag{18}$$

$$\left.\frac{\partial v_i(M_i,M_{i+1})}{\partial y_i}\right|_{y_i=\frac{b_i}{2}} = \left.\frac{\partial v_{i+1}(M_{i+1},M_{i+2})}{\partial y_{i+1}}\right|_{y_{i+1}=\frac{-b_{i+1}}{2}} \tag{19}$$

(i=2,3,4,5 , when i=5， i+2=1)

Eqs.(17)-(19) are equivalent to Eqs.(20)-(22)

$$E_{6m}\frac{1}{D_6}(F_{6m}-H_{6m})+E_{1m}[\frac{1}{D_6}(F_{6m}+H_{6m})+\frac{1}{D_1}(F_{1m}+H_{1m})]+E_{2m}\frac{1}{D_1}(F_{1m}-H_{1m})=\frac{4\pi}{a}\sum_{m=1}^{\infty}\frac{m}{\sin\frac{m\pi x}{a}}\left(\frac{\partial v_1(q)}{\partial y}\right)\Big|_{y_1=0} \tag{20}$$

$$E_{1m}\frac{1}{D_1}(F_{1m}-H_{1m})+E_{2m}[\frac{1}{D_1}(F_{1m}+H_{1m})+\frac{1}{D_2}(F_{2m}+H_{2m})]+E_{3m}\frac{1}{D_2}(F_{2m}-H_{2m})=-\frac{4\pi}{a}\sum_{m=1}^{\infty}\frac{m}{\sin\frac{m\pi x}{a}}\left(\frac{\partial v_1(q)}{\partial y}\right)\Big|_{y_1=b_1} \tag{21}$$

$$E_{im}\frac{1}{D_i}(F_{im}-H_{im})+E_{(i+1)m}[\frac{1}{D_i}(F_{im}+H_{im})+\frac{1}{D_{i+1}}\times(F_{(i+1)m}+H_{(i+1)m})]+E_{(i+2)m}\frac{1}{D_{i+1}}(F_{(i+1)m}-H_{(i+1)m})=0 \tag{22}$$

(i=2,3,4,5 ,when i=5 , i+2=1)

Eqs. (20), (21) and (22) form m sets of equations. In each set of equations, there are 6 equations and there are also 6 unknown variables (E_{1m}, $E_{2m}\cdots E_{6m}$), therefore these sets of equations have unique solutions. And the bending moments (M_1, $M_2\cdots M_6$) of each plates could also be obtained. Subsequently, the deflection equations of each plates could be derived. We can then calculate the surface stress of each plate from the known deflection equations using the following equations:

$$\sigma_x^{"}=\frac{E\delta}{2(1-\mu^2)}\left(\frac{\partial^2 w}{\partial x^2}+\mu\frac{\partial^2 w}{\partial y^2}\right) \tag{23}$$

$$\sigma_y^{"}=\frac{E\delta}{2(1-\mu^2)}\left(\frac{\partial^2 w}{\partial y^2}+\mu\frac{\partial^2 w}{\partial x^2}\right) \tag{24}$$

$$\tau_y^{"}=\frac{E\delta}{2(1+\mu)}\frac{\partial^2 w}{\partial x\,\partial y} \tag{25}$$

Substituting Eqs. (23), (24) and (25) and (6) into the Eqs. (1), (2) and (3), the stress components (σ_x, σ_y and τ_{xy}) at any locations of the out surface of the out booms can be derived.

Both the theory and the method of calculation of the local bending stress for the inner booms are identical to those of the out booms. Therefore the corresponding equations are not given in this paper for the sake of brevity.

III. VALIDATION OF THE ANALYTICAL MODEL

A. Parameters of the Boom Geometry and Materials

To validate the accuracy of the analytical model developed in this paper, both experiments on a real telescopic boom structure and finite analyses have been carried out. The structure used to perform the experiment and analyses is the telescopic boom on a typical aerial work platform. The geometric data of the telescopic boom system are given in Table 1.

The extension lengths and the lengths of the overlapping contact regions of the telescopic booms are: l_3=5420mm, l_2=4890mm, l_1=4975mm, x_3=800mm, x_2=1050mm, x_1=1100mm. The payload P_N=330Kg. The length of the sliding block u_1=150mm, Young's modulus of the material E=2.1×105(MPa), Poisson ratio μ=0.3, and the density of the steel material ρ=7.85×10^{-6}(Kg/mm^3).

TABLE 1. THE DIMENSIONS OF THE CROSS-SECTION

Parameter of Cross Section	First Boom	Second Boom	Third Boom
H/mm	334	286	241
W/mm	266	232	200
H_1/mm	280	240	195
W_1/mm	120	100	80
T/mm	5	4	4
α/°	125	125	125

B. Experiment

The aerial work platform used for the test is shown in Fig.12. The pictures showing the strain gauges on the surface of the tested boom are given in Fig.13, and the distribution of the measurement points are illustrated in Fig.14. The base point of the measurement, a, is located on the symmetric line of the surface of top flange of the first boom, and just above the upper sliding block of the second boom, see Fig.14. The locations of the rest nine strain gauges are determined by the relative distances to this base point.

During testing, the telescopic boom was kept at horizontal position and all its component booms were fully extended. This is one of the most critical loading cases. When the telescopic boom was operated under this

configuration, the reaction forces on the sliding blocks are maximum. The payload of P_N=2KN was lifted from the ground. After the boom was held in this testing position for about 10s, the vibration of the boom was found to be not obvious and then the strain gauge values were read and recorded. The stress components in the x and y directions were measured separately.

Figure 12. A typical aerial work platform

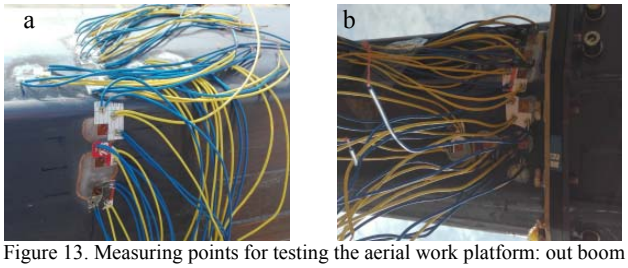

Figure 13. Measuring points for testing the aerial work platform: out boom (left) and inner boom (right).

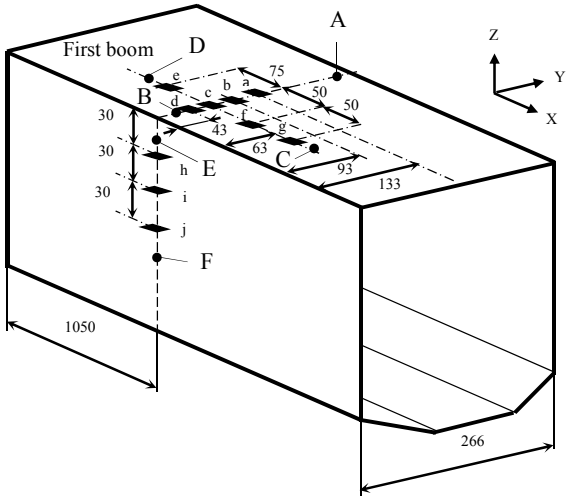

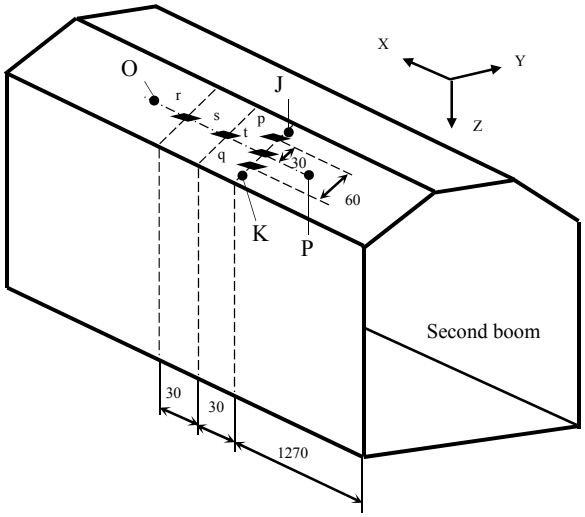

Figure 14. Layout of measuring points: out boom (top) and inner boom (bottom).

C. *Finite Element Analysis*

In order to further verify the accuracy of the analytical model developed, an more accurate finite element model has been develop. The finite element mesh is shown in Fig.15. To avoid the modeling error caused by the structural geometric simplification, the whole upper carriage structure was included in the finite element models. To increase the analysis accuracy, solid brick elements were used throughout. Contact elements were used to simulate the realistic contact behavior at the overlapping regions between neighboring booms.

The Mises equivalent stress distribution at the overlapping contact zone of the first and second telescopic boom components from the finite element analysis is given in Fig.16. The contour plots of stress components in the vicinity of the local contact region is given in Fig. 17.

Figure 15. Finite element mesh for the telescopic boom

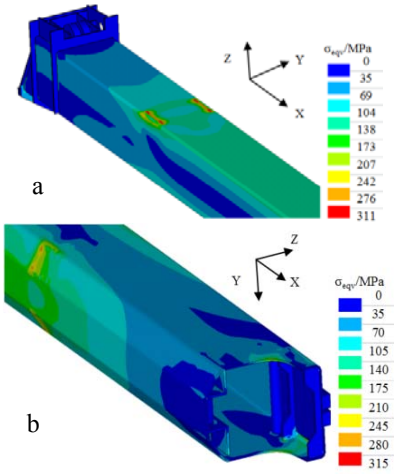

Figure 16. Mises equivalent stress in the contact zone: out boom (top) and inner boom (bottom).

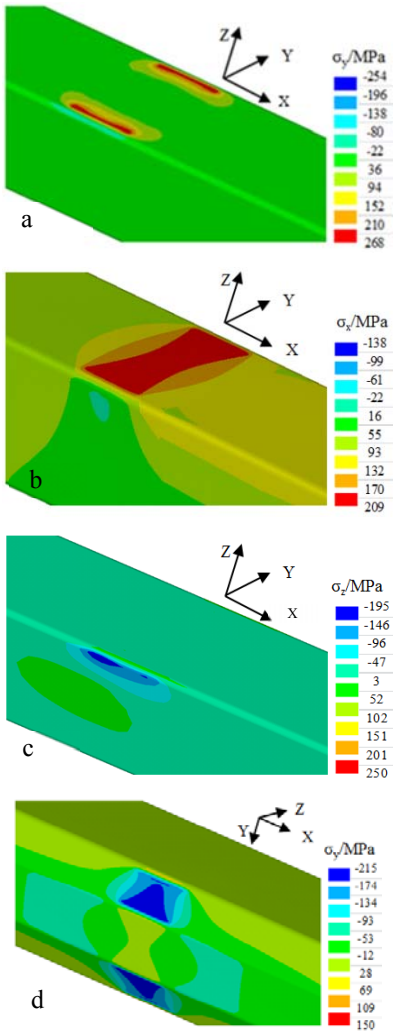

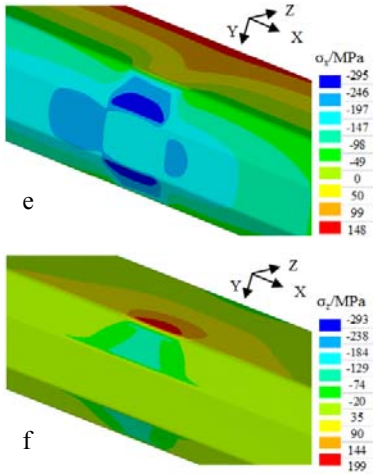

Figure 17. a Stress in y direction of first boom,
b Stress in x direction of first boom,
c Stress in z direction of first boom,
d Stress in y direction of second boom,
e Stress in x direction of second boom,
f Stress in z direction of second boom.

D. Comparison of Models and Experimental Validations

The stress analysis results from two theoretical models, solid finite element model (FEM) and experiment data are all compared in detail in this section. The first theoretical model presented is the traditional analytical model (labeled as Traditional analysis in the graphs) which uses the assumption that the contact occur on the whole surface of the contact sliding blocks. The second theoretical model is the one newly proposed in this paper (labeled as New model in the graphs), which using the assumption that the contacts occur only on the narrow edge areas of the sliding blocks.

Fig.18 shows stress distribution along a transverse path line AB (as marked in Fig.(14a)) on the top flange plate of the first boom. Fig.19 shows stress distribution along a longitudinal path line CD (see Fig.(14a)) on the top flange plate of the first boom. Fig.20 shows stress distribution along a transverse path line EF (see Fig.14(a)) on the vertical web plate of the first boom. Fig.21 shows equivalent stress distribution along a transverse path line JK (see Fig.14(b)) on the inclined web plate of the second boom. Fig.22 shows equivalent stress distribution along a longitudinal path line OP (see Fig.14(b)) on the inclined web plate of the second boom. From all these comparison figures, it can be seen that the results from the new model correlate excellent well with those from both the accurate solid finite element analysis and the experimental data. However the traditional analysis shows significant discrepancies, which means that the widely used assumption that the contact pressures are evenly distributed on the entire surface of the sliding block is not rational and the use of it may lead to significant errors in predicting stress in the telescopic boom structures. The new assumption that the contacts occur only on the narrow edge

areas of the sliding blocks, derived from the observation from the accurate FEM analysis results is rational and the newly proposed analytical model based on it can yield very accurate stress prediction.

The maximum equivalent stress appears on the top flange plate of the first telescopic boom, the maximum equivalent stress value calculated from the new model is σ_e=250.8 (MPa). The equivalent stress at this location from experimental testing and FEM analysis are σ^T_e=262.8 (MPa), and σ^E_e=246.5 (MPa), respectively. The maximum relative differences of equivalent stress at this location between the newly proposed theory and both of the experimental results and accurate FE analysis are less than 4.6%.

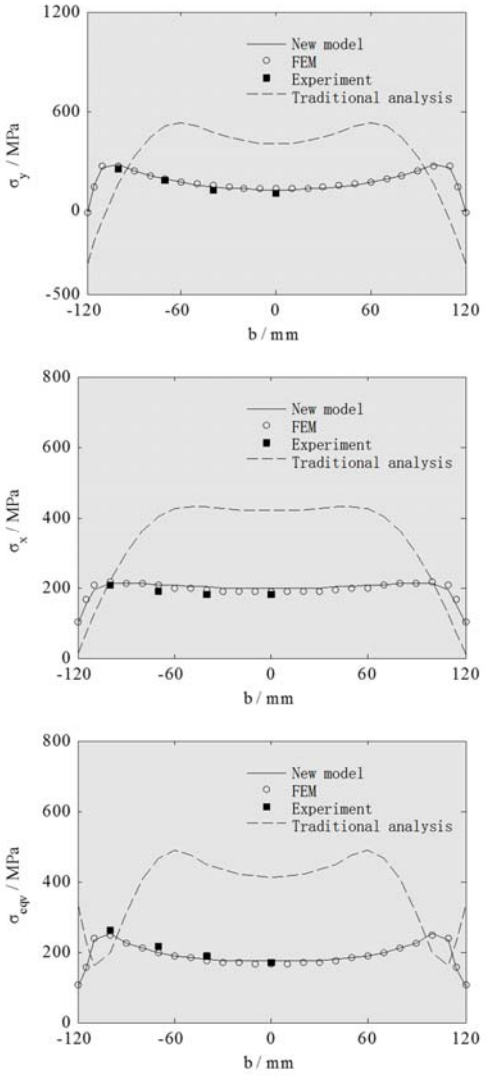

Figure 18. Comparison of stresses along path AB on the first boom: σ_y (top), σ_x (mid) and σ_{eqv} (bottom)

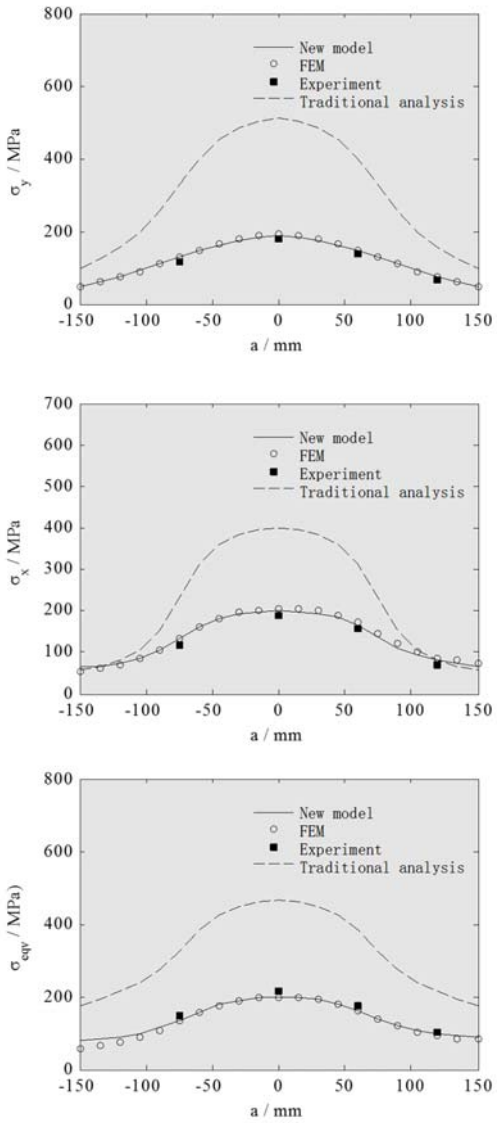

Figure 19. Comparison of stresses along path CD on the first boom: σ_y (top), σ_x (mid) and σ_{eqv} (bottom).

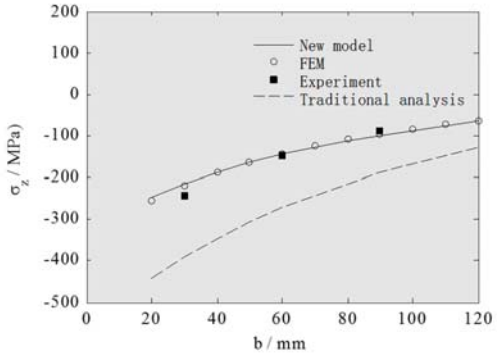

Figure 20. Comparison of σ_z stress along path EF on the first boom

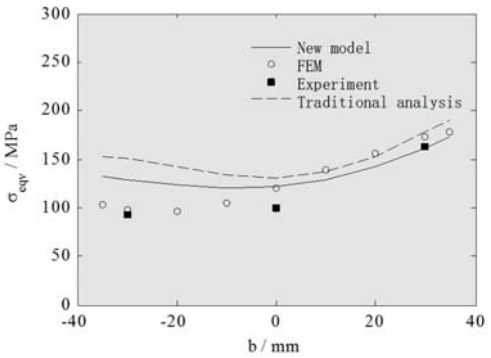

Figure 21. Comparison of Mises stresses along path of JK on the second boom

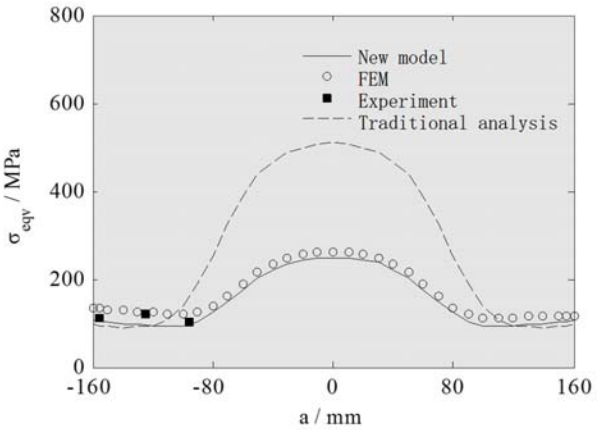

Figure 22. Comparison of Mises stresses along path of OP on the second boom.

IV. CONCLUSIONS

A mathematical model has been proposed for the efficient and accurate analysis of stresses in the contact zones of telescopic boom structure. According to the principle of superposition, the total stress can be calculated as superposition of the global longitudinal bending stress and the local lateral bending stress. For the local stress analysis model, a new assumption has been proposed on the contacts between the adjacent booms. The new model assumes that the contacts only occur on very narrow areas along the edges of the sliding blocks, and this assumption has been justified from the accurate finite element analysis. Numerical results show that the conventional analysis based on the assumption of uniform stress distribution on the entire surface of the sliding block predict far too high a stress level. Whilst the results from the new model based on the narrow local contact assumption are in good agreement with both the finite element analysis and carefully conducted experimental results on a real telescopic boom structure of an aerial work platform.

ACKNOWLEDGMENTS

This work was supported by the National Natural Science Foundation of China (Grant No. 51375420), Hebei Natural Science Research funding under grant E2015203196.

REFERENCES

[1] Z. M. Li, "Stress analysis of the sliding blocks on the telescopic boom and the research of its character," Master Thesis, Southwest jiaotong university, China, 2009.

[2] Y. Z. Cai, "Research on cross-sections and size optimization of modern telescopic boom," Master Thesis, Dalian university of technology, China, 2012.

[3] B. S. Liu, J. N. Wang, "Calculation of local stress at the sliding shoe of the telescopic boom of a truck crane," Hoisting and Conveying Machinery, pp. 14-18, May, 1994.

[4] M. Djelosevic, V. Gasic and D. Petrovic, "Identification of local stress parameters influencing the optimum design of box girders," Engineering structures, vol. 40, pp. 299-316, 2012.

[5] M. Savkovic, M. Gasic and G. Pavlovic, "Stress analysis in contact zone between the segments of telescopic booms of hydraulic truck cranes," Thin-Walled Structures, vol. 85, pp. 332-340, 2014.

[6] H. Shao, Q. Feng and S. L. Zhang, "Finite element analysis on telescopic boom of an aerial work platform with different modeling methods," Construction Machinery and Equipment, vol. 39, pp. 26-30, 2008.

[7] Y. S. Ren, X. J. Yu and Z. P. Zhou, "Finite element calculation and optimal design of the telescopic arm of crane," Journal of Changchun Institute of Technology(Natural sciences edition), vol. 8, pp. 34-36, 2007.

[8] Z. W. Chen, Z. Cui and W. G. Jiang, "Structural optimization of the telescopic boom of a certain type of truck-mounted crane," Applied Mechanics and Materials, vol. 548, pp. 383-388, 2014.

[9] X. Lin, "Analysis of contact problems and study of regularity on telescopic boom's sliders," Master Thesis, Dalian university of technology, China, 2011.

[10] J. Z. Hea, and Y. Chenb, "Analysis and Optimal Design about a kind of Bearing Beam with Sleeve Joint Structure," Procedia Environmental Sciences, pp. 275-280, November 2011.

[11] W. Wang, Q. H. Yu and J. R. Zhang, "Application of the Theory of Elastic Thin Plate in the Mechanical Analysis of Box Girder," Journal of Changsha communications university, vol. 20, pp. 60-64, April 2004.

[12] S. Timoshenko and S. Woinowsky, "Theory of plates and shells," Beijing:Science Press, 1997.